Spin charging sequences in three colinear laterally coupled vertical quantum dots

J. Kim, D. V. Melnikov, and J. P. Leburton
Beckman Institute for Advanced Science & Technology and Department of Electrical and Computer Engineering, University of Illinois at Urbana-Champaign, 405 N. Mathews Avenue, Urbana, Illinois 61801, USA

D. G. Austing
Institute for Microstructural Sciences, National Research Council of Canada, 1191 Montreal Road, Ottawa, Ontario, Canada K1A 0R6

S. Tarucha
Department of Applied Physics, University of Tokyo, Hongo, Bunkyo-ku, Tokyo 113-0033, Japan
(Received 22 November 2005; revised manuscript received 15 March 2006; published 11 July 2006)

The electronic properties of three colinear and laterally coupled vertical quantum dots are investigated by three-dimensional self-consistent simulations based on the density functional theory within the local spin density approximation. From a simulation viewpoint, it is shown that the physical dimensions of experimentally realizable mesa structures should be optimized to produce equal size quantum dots. Single electron charging sequences are studied as a function of two sets of gate voltage configurations, i.e., center gate variation on the center dot mesa and side gate variation on the two outer dot mesas, separately. In the former, electrons are shown to relocalize from the outer dots to the center dot with the onset of a spin-density wavelike profile for three and four electrons, respectively. In the latter, double charging is seen to take place with the onset of localization in each of the outer dots for $N=3$ and $N=4$ electrons. Finally, we obtain the stability diagram of the system, showing features specific to the colinear triple quantum dots (TQD) coupling.

DOI: 10.1103/PhysRevB.74.035307 PACS number(s): 73.21.−b, 72.20.My, 73.40.Gk

I. INTRODUCTION

As the size of electronic device dimensions decreases, quantum effects become more prominent and interfere with conventional device operation.[1] With these phenomena looming ahead in the near future, there is a growing interest in exploiting quantum effects in new paradigms for information processing, for which classes of problems previously deemed to be intractable can be solved expediently with a quantum computer.[2,3] In quantum computing, the basic unit of information is a quantum bit or qubit (i.e., a quantum object, such as the electron spin), which can be represented by a superposition of two unit vectors in the two-dimensional (2D) Hilbert space. At the hardware level, it has been demonstrated that a Controlled-NOT (CNOT) gate and a single qubit gate are the universal building blocks to obtain all quantum logical functions.[4] Coupled quantum dots (QDs) are promising systems for realizing CNOT gates and moreover, entanglement between two electron spin qubits can be manipulated by external electric and magnetic fields.[5]

Beyond two coupled QDs, the next obvious step, three coupled QDs arranged either in a linear array or in a triangular formation can give extra functionality. Such devices, such as a solid-state entangler,[6] a charging rectifier,[7] a coded qubit,[8] and quantum gates,[9] have recently been proposed to utilize triple QD structures, providing incentives to investigate these systems. Moreover, from a fundamental physical viewpoint, the triple QD system presents great interest as an artificial triatomic molecule where the interplay between geometrical confinement, interdot coupling, and many-body effects offers a rich variety of phenomena, which have not yet been investigated extensively.

In this paper, we study theoretically the few-electron properties of three laterally coupled vertical quantum dots (TQDs). This structure offers the advantage of the modulation of the interdot coupling potential with tuning gates, and the control of electron confinement within each of the three dots with a separate set of gates. We use density functional theory within a self-consistent local spin density approximation (LSDA) to model the electronic properties of TQDs. In this context, we provide design guidelines for optimizing the structure for operation with realistic sets of voltage values, which for the few-electron regime are often difficult to access experimentally. We then obtain the spin configurations of a few electrons for different combinations of interdot coupling and intradot confinement. We also derive the charging diagrams for two potential configurations resulting from the interplay between the three sets of gates. In particular, we show that cross capacitances between tuning and confining gates that are often theoretically neglected[10] impose important conditions on the charging and electron spin configurations in the TQD system. We finally show that the charge stability diagram obtained with this kind of TQD structures is totally different from those observed in double quantum dot systems.

In Sec. II we describe the vertical TQD structures currently being pursued experimentally. The self-consistent computational approach based on the multiscale, spin density functional theory,[11] used to simulate the TQD structure and for which the electrostatic potential is obtained by the device boundary conditions from the Poisson equation is presented in Sec. III. In Sec. IV we provide the results of our simulations. Finally, in Sec. V we summarize the important points mentioned in the paper and discuss future work.

II. VERTICAL TRIPLE QUANTUM DOT STRUCTURE

A scanning electron microscope image of a typical colinear TQD structure under investigation is shown in Fig.

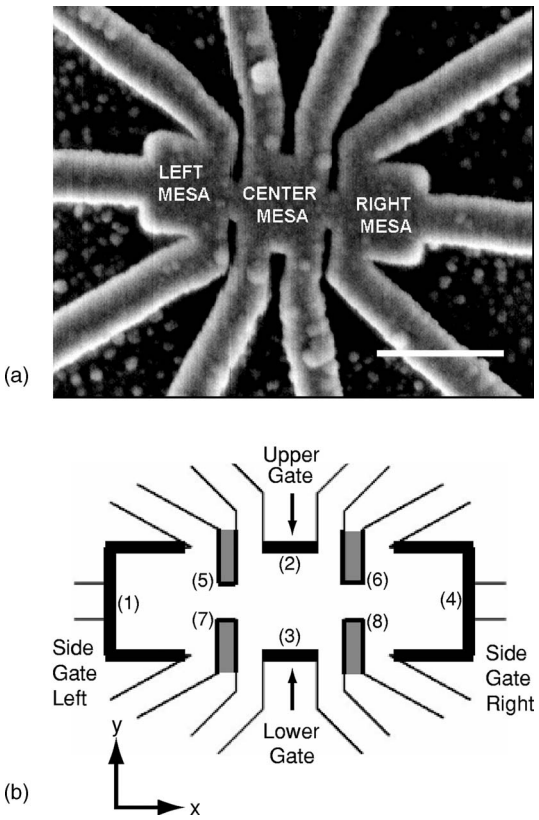

FIG. 1. (a) Scanning electron microscope image of a typical three laterally coupled vertical quantum dot structure under investigation (scale bar 1 μm). A QD is located in each of the three square mesas. The ten thin line mesas radiating from the central three-mesa structure carry metal contact wires and keep separate each of the gates. (b) Also shown is a schematic top view of the TQD structure modeled. The four confining gates (represented by thick lines) are numbered (1)–(4), and the four tuning gates (represented by gray-shaded rectangles) are numbered (5)–(8).

1(a).[12] This structure builds on the recent successful fabrication and operation of its two dot cousin,[13] which, in turn, arose out of a new approach for multiple gating of single vertical dots.[14] Figure 1(b) shows the top view of the TQD structure in the x-y plane. Numbers (1)–(4) in Fig. 1 indicate the location of the four confining gates. Starting from top of the TQD structure, these gates protrude all the way down almost to the $In_{0.055}Ga_{0.945}As$ semiconductor layer along the z direction (see Fig. 2 for the vertical cross section). The confining gates on the three square mesas primarily provide the electrostatic fields that create the quantum dots and also control the number of electrons in each of the dots.[15] Voltage variations on these gates determine the conditions for single electron charging in each QD. The size of the three square dot mesas is initially taken to be 0.6 μm$\times$0.6 μm in the x and y directions. Located in the middle of the device structure, in between adjacent dot mesas, are four tuning gates [numbers (5)–(8) in Fig. 1] also protruding down toward the $In_{0.055}Ga_{0.945}As$ layer. These gates effectively separate the individual QDs from each other by inducing energy barriers between the QDs. Hence, exchange coupling between electrons in each QD can be controlled by changing the voltage

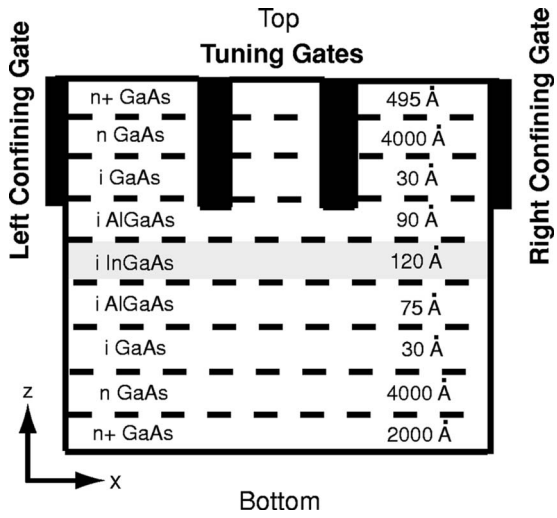

FIG. 2. Cross-sectional view of the vertical TQD structure showing the layered structure. The confining and the tuning gates are shown in solid black. The location of the $In_{0.055}Ga_{0.945}As$ quantum well is indicated by the shaded region.

bias on the tuning gates. The tuning gates were initially designed to be 0.1 μm$\times$0.2 μm in the x and y directions, but as seen in the results section (IV), these sizes have been changed in order to optimize the structure. The ten thin line mesas emerging from the central three-mesa structure containing the TQDs carry metal contact wires from the top of the semiconductor (for Ohmic contacts) to large bonding pads (not shown) and keep separate each of the gates (1)–(8).[12] In our model, we essentially ignore these thin line mesas, and the bonding pads, as well as the Ohmic contacts, and this makes the overall simulation region rectangular.

Figure 2 shows a vertical cross section of the layered structure cut across the tuning gates along the x direction. The total depth of the simulated structure is 1.084 μm along the z direction as obtained from the succession of the various layer thicknesses in the designed semiconductor material. At the bottom (the substrate side) of the simulated structure, there are four n-doped GaAs layers ($n+=2\times10^{18}$ cm^{-3}, $n=2\times10^{17}$ cm^{-3}, $n=1.4\times10^{17}$ cm^{-3}, and $n=1.0\times10^{17}$ cm^{-3}), each of them 2000, 1800, 1500, and 700 Å wide, respectively. Next there is a 30 Å undoped GaAs layer, and then there is the $Al_{0.20}Ga_{0.80}As$-$In_{0.055}Ga_{0.945}As$-$Al_{0.20}Ga_{0.80}As$ double barrier structure with layer thicknesses of 75, 120, and 90 Å, respectively. Our main interest is in this central quantum well region, since electron charging and localization in the three QDs occurs in the $In_{0.055}Ga_{0.945}As$ layer in the presence of the lateral confinement imposed by gates (1)–(8). Above this double barrier structure, there is another undoped 30 Å GaAs layer, and above that four doped GaAs layers with the same dopant densities as the doped layers below the double barrier structure. Note the upper $n+$ layer on top of the layered structure facilitates Ohmic contacts.

III. COMPUTATIONAL MODEL

Owing to the three-dimensional (3D) geometry of the TQD structure, we use a 3D self-consistent quantum device

computational model to describe the experimental system as realistically as possible. Since it is well known that 2D models overestimate electron-electron interaction due to the reduction of the electron motion in a plane instead of in a volume, the 3D Kohn-Sham equations coupled with the 3D Poisson's equation are well suited to obtain the self-consistent electrostatic potential as well as the stable electron charge and spin density distributions as a function of the applied gate voltages.[16] Our approach is based on the spin density functional theory (SDFT) within the effective mass approximation to describe the many-body effects among the conduction electrons in the TQD structure. The Kohn-Sham equations, one for spin up and the other for spin down, read as follows:

$$H^{\uparrow}(\vec{r})\psi_i^{\uparrow}(\vec{r}) = \varepsilon_i^{\uparrow}\psi_i^{\uparrow}(\vec{r}), \quad H^{\downarrow}(\vec{r})\psi_i^{\downarrow}(\vec{r}) = \varepsilon_i^{\downarrow}\psi_i^{\downarrow}(\vec{r}), \tag{1}$$

where the respective Hamiltonians are expressed as

$$H^{\uparrow(\downarrow)}(\vec{r}) = -\frac{\hbar}{2}\nabla\left[\frac{1}{m(\vec{r})}\nabla\right] - q\phi(\vec{r}) + \Delta E_c + \phi_{Xc}^{\uparrow(\downarrow)}(n). \tag{2}$$

$m^*(\vec{r})$ is the position-dependent effective mass, and the electrostatic potential $\phi(\vec{r}) = \phi_{\text{ext}} + \phi_{\text{ion}} + \phi_H$, where ϕ_{ext} is the potential due to externally applied bias, ϕ_{ion} the potential resulting from the ionized donors, and ϕ_H the Hartree potential accounting for the repulsive electron-electron interactions. ΔE_c is the conduction band offset resulting from the boundaries between two different materials. ϕ_{xc} is the exchange-correlation potential for spin up and spin down electrons, computed within the local spin density approximation (LSDA).[17] The electrostatic potential $\phi(\vec{r})$ is obtained by solving the Poisson's equation

$$\nabla[\varepsilon(\vec{r})\nabla\phi(\vec{r})] = -\rho(\vec{r}), \tag{3}$$

where $\varepsilon(\vec{r})$ is the position-dependent permittivity and $\rho(\vec{r})$ is the total charge density given by the following:

$$\rho(\vec{r}) = q[p(\vec{r}) - n(\vec{r}) + N_D^+(\vec{r}) - N_A^-(\vec{r})], \tag{4}$$

where $N_D^+(\vec{r})$ and $N_A^-(\vec{r})$ represent the ionized donor and acceptor concentrations in the device layers, $p(\vec{r})$ is the total hole concentration level, and $n(\vec{r})$ is the total electron density in the TQD region

$$n(\vec{r}) = n^{\uparrow}(\vec{r}) + n^{\downarrow}(\vec{r}) = \sum_{i=1}^{N\uparrow} |\psi_i^{\uparrow}(\vec{r})|^2 + \sum_{i=1}^{N\downarrow} |\psi_i^{\downarrow}(\vec{r})|^2 \tag{5}$$

with $N\uparrow + N\downarrow = N$ being the total number of electrons in the dot. Since we are dealing with n-type semiconductor layers at low temperature, we set both $N_A^+(\vec{r})$ and $p(\vec{r})$ to be zero.

The TQD simulation region is divided into two separate regions: the QD region in which quantum mechanical effects predominate and a larger scale bulk region in which the free electron concentrations are described by semiclassical statistics. This multiscale approach provides a realistic description of the confining potential, while relating directly gate voltage variations with the stable charge and spin configurations in the TQD system. The temperature is $T=0$ K in the QD region, while it is set to be 1.5 K in the semiclassical regions for numerical convergence purposes. This temperature difference between the two regions is inconsequential for the accuracy of the computation. We impose the zero-normal field Neumann boundary conditions on the top of the TQD structure as well as on the sides below the confining and tuning gates. The Schottky barrier Φ_S^0 value is taken into account and added to the applied gate bias for the boundary conditions on the metal-semiconductor interfaces $(-q\phi_S^0 - qV_G)$ with $\phi_S^0 = -0.8$ V and V_G as the applied gate bias. Finally, we set the potential to be zero on the bottom surface of the simulated structure. We assume the electron wavefunctions vanish outside the QD region and accordingly restrict our simulation domain for solving the KS equations. $(155 \times 41 \times 77)$ grid points are used to discretize the nonuniform mesh with the majority of these points assigned to the TQD region.

In our simulations, the system of Eqs. (1)–(4) is solved iteratively until the self-consistent solution of the single particle orbitals and eigenvalues are obtained. Although the finite difference method is the most popular method to discretize the Kohn-Sham and Poisson's equations, we use the finite element method (FEM) with trilinear polynomials to perform the self-consistent process[18] because it is more convenient for complex geometries.[19] The discretized Poisson equation is solved using the damped Newton-Raphson method[20,21] while the generalized eigenvalue problem obtained as a result of Kohn-Sham equation discretization is approached by means of a subspace iteration method based on a simple Rayleigh-Ritz analysis.[22]

In order to determine the stable electron and spin configurations, one can use Slater's Formula,[23] which is also useful in determining the QD charging voltages from $N-1$ to N electrons. However, in our case the Slater's Formula ultimately gives unphysical results for $N=1$. As a result, we chose to calculate the total energy of the system, which consists of the following components:

$$E_{\text{Total}} = \sum_{i=1}^{N} \varepsilon_i^{\uparrow} n_i^{\uparrow} + \sum_{i=1}^{N} \varepsilon_i^{\downarrow} n_i^{\downarrow} - \frac{\varepsilon_H}{2} + \varepsilon_{xc} - \varepsilon_{xc\_\text{pot}}, \tag{6}$$

where $\varepsilon_I^{\uparrow\downarrow}$ is the eigenenergy value for state i, ε_H is the Hartree energy, ε_{xc} is the exchange-correlation energy, and $\varepsilon_{xc\_\text{pot}}$ is the exchange-correlation potential energy. By comparing the total DFT energy of the system for different number of electrons, the charging of the TQD from $N-1$ to N electrons can be determined by looking for crossing points in the different energy curves. In our simulations, the Fermi energy is taken to be zero.

IV. RESULTS

A. TQD structure optimization

The conduction energy band along the x direction for the original TQD structure described in Sec. II is shown in Fig. 3 (lower trace). The confining gates are set to −1.7 V and the tuning gates to 0 V for this particular plot. Analyzing the plot, we identify three potential problems: (i) The calculated ground-state energy level is found to be 28 meV below the Fermi energy level, which implies that for this gate bias con-

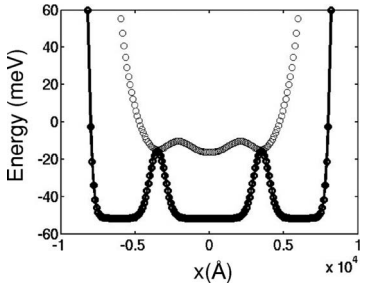

FIG. 3. Conduction energy band along the x direction for the original structure (lower trace) and the optimized structure (upper trace). For the optimized structure: (i) the length of the tuning gates along the y direction has been reduced to 0.1 μm; (ii) the center dot mesa size has been reduced to 0.3 μm in the x direction, and the two outer dot mesas have been increased in size by 0.05 μm along the x direction; and (3) the dopant concentration of the first 700 Å of the n-GaAs layer located just above and below the central undoped layers has been reduced from 10^{17} to 10^{16} cm^{-3}.

figuration the QDs already contain many electrons. In order to start the charging process from the first electron, the ground-state energy level should be within a few millielectron volts of the Fermi energy level. By making the confining gate biases more negative, the energy levels move up, which can potentially fix our problems. However, due to the possible presence of reverse-biased leakage currents at gate biases around −3.0 to −2.5 V, this option should be avoided.[12] (ii) The energy barrier separating adjacent quantum dots (around 40 meV) is too high in the initial gate bias configuration, which prevents significant quantum mechanical coupling between the dots. Ideally, we would like the barrier height to be around 5–10 meV. To remedy this situation, the bias of the tuning gates should be made more positive. Since the tuning gates are already set at 0 V, the Schottky barrier at the metal-semiconductor interfaces of the tuning gates will be forward biased, and this too can eventually induce undesirable current leakage through the gates.[12] (iii) Lastly, the three dots have unequal sizes due to an inherent asymmetry unintentionally built into the design of this particular TQD structure. Indeed, examining the conduction energy band edge in Fig. 3, the two side dots appear smaller along the x direction compared to the center dot. This is due to the overly strong confining effect of the large side gates [numbers (1) and (4) in Fig. 1(b)], while the center dot is only controlled by the relatively short center gates [numbers (2) and (3) in Fig. 1(b)]. In some device proposals for linear TQD structures, the center dot is made relatively small to create a large spacing between the different energy levels.[24] For instance, in a solid-state entangler,[6] a spin-singlet state is first prepared in the center dot, for each electron to be then transported to the two side dots without loss of entanglement. However, if the energy spacing in the center dot is too small due to its large size, it could be very difficult in practice to maintain the electrons in their ground state since small thermal energy excitations could destroy the ground state.

Because of the aforementioned problems arising in the original structure design, the structure should be changed in an optimal way to remedy these shortcomings. The length of the four tuning gates along the y direction has been reduced from 0.2 to 0.1 μm, which reduces the overall effect of the tuning gates, resulting in a decrease in the interdot barrier height. We have also decreased the nominal width of the center mesa to 0.3 μm, while increasing the nominal width of the two outer mesas by 0.05 μm in order to equalize the size of the dots. Finally, we have decreased the dopant concentration in the two adjacent n-doped GaAs layers, located just above and below the central undoped layers, from 10^{17} to 10^{16} cm^{-3} in order to raise the ground-state eigenenergy levels closer to the Fermi energy level. The conduction energy band of the newly modified optimized structure along the x direction is shown in Fig. 3 (upper trace). The left and the right confining side gates are set at −2.4 V, the upper and the lower confining gates at −2.1 V, and the tuning gates at −0.05 V. For this particular configuration, the barrier height level between the dots is ~5 meV.

B. Single electron charging

Single electron charging in the TQD structure can be achieved by bias variation of either the center confining gates or the side confining gates.

1. Center gate charging

Figure 4(a) shows the electron charging diagram for the first four electrons added to the TQD structure where the total energy of the N-electron system is plotted with respect to the bias on gates (2) and (3). For these simulations, the upper and the lower center confining gates are jointly varied, making the overall system symmetric. The side confining gates (1) and (4) are set to a constant −2.4 V, and the four tuning gates are maintained at −0.05 V throughout the charging process. The dashed line indicates the Fermi energy level, which as mentioned earlier is set to 0 meV. We compute four different curves corresponding to $N=1$, 2, 3, and 4 electrons in the TQD.

All four curves in Fig. 4(a) are characterized by two regimes: when the gate bias on (2) and (3) is most negative, the curves are nearly flat with the total energy value increasing with the number N of electrons, except for $N=1$, which is between the $N=2$ and $N=3$ curves, while at more positive gate bias, the slopes become strongly negative and the order of the curves with respect to N reverses, with an abrupt transition at intermediate voltages. This latter feature can be attributed to a relocalization of electrons from the two side dots to the center dot under the influence of the bias on the two center gates [see Fig. 4(b)]. At very negative bias the electrons are localized in the two side dots, which are at lower potential energy ($V_{CCG}=-2.4$ V) than the center dot ($V_{CCG}<-2.4$ V); therefore changes of the two center gate voltages do not exert much influence on the total energy of the system in this regime since these gates are more physically decoupled from the electrons located in the two side dots. As a result, the total energy curves are characterized by only a slight negative slope. As the bias on gates (2) and (3) is made more positive than $V_{CCG}=-2.4$ V (fixed side gate voltage), there is a point where the potential well of the center dot becomes lower than the potential wells of the side dots, and electrons relocalize into the center dot, resulting in

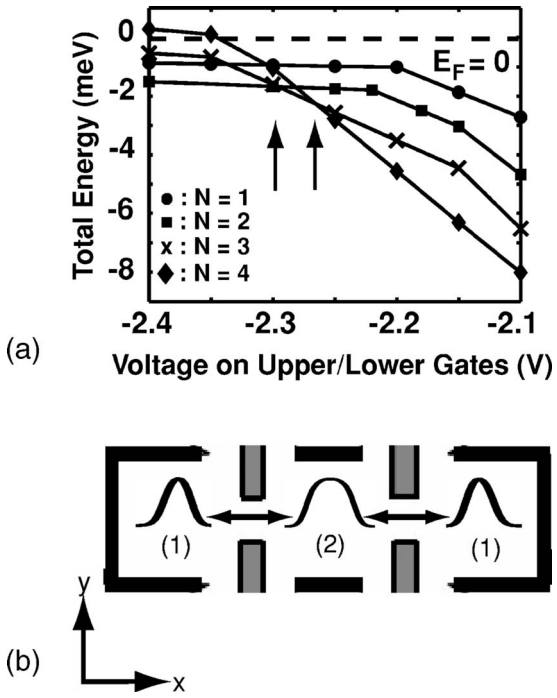

FIG. 4. (a) Electron charging diagram for the first four electrons. The Fermi energy is indicated by the horizontal dashed line at 0 meV. The four curves represent the total energy of the whole QD system containing $N=1$ to $N=4$ electrons at different upper/lower gate biases. The two arrows indicate points in which electrons are added to the system ($N=2\rightarrow N=3$) and ($N=3\rightarrow N=4$). (b) Schematic representation of two different configurations for the ground state of the two-electron wave functions. For center confining gate (CCG) biases $V_{CCG}<-2.24$ V, the electrons are localized in the two outer dots (1). Upon making the voltage of these gates more positive, the electrons relocalize into the center dot (2).

their closer physical proximity to the two center gates. Hence in this new arrangement, the total energy of the system becomes much more sensitive to changes made to the center gate biases, so reflecting in more negatively sloped curves. Hence, for $N=1$ and for $V_{CCG}<-2.2$ V, the electron wave function is localized separately in the two side dots, which is simply interpreted as meaning a 50% probability of localizing the electron in either the left side dot or the right side dot, while the electron occupies the center dot for $V_{CCG}>-2.2$ V. For $N=2$ one electron is localized in one of the two outer dots, whereas at a bias more positive than −2.15 V, they both occupy the center dot where their energy is a strong function of V_{CCG} [see Fig. 4(b)]. Transitions occur between −2.24 and −2.15 V, where wave function hybridization between the side dots and center dots occurs. From a numerical point of view, our simulations did not converge in this range as in the self-consistent approach: the two electrons just oscillate back and forth from the side dots to the center dot at each iteration.

For $N=3$ and for biases more negative than −2.35 V, all electrons are in the side dots (the two ↑ electrons are located one in each of the side dots in degenerate single-particle states and the ↓ electron is shared between the two side dots with an energy level about 0.4 meV above the degenerate state). Between −2.35 and −2.15 V, the ↓ electron occupies

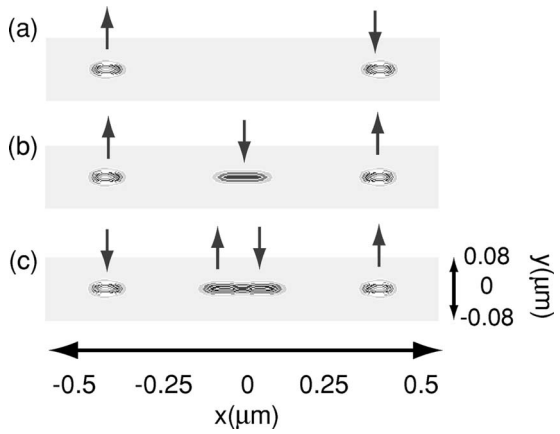

FIG. 5. Ground-state electron densities for (a) $N=2$, (b) $N=3$, and (c) $N=4$ electrons. The arrows indicate the spin orientation. (a) $V_{CCG}=-2.35$ V: the two electrons are localized in the two outer dots. (b) $V_{CCG}=-2.3$ V: two spin up electrons and one spin down electron form the ground-state configuration. (c) $V_{CCG}=-2.25$ V: for four electrons, a two-electron singlet is formed in the center dot.

the center dot while the two ↑ electrons remain in the side dots. For biases $V_{CCG}>-2.15$ V, all three electrons eventually fall into the center dot with a s^2p^1 configuration.

For $N=4$ and for biases more negative than −2.35 V, two-electron singlets occupy the two side dots. Above $V_{CCG}=-2.35$ V, two electrons occupy the center dot and two electrons remain in the side dots, one in each. For $V_{CCG}\gg-2.35$ V, all four electrons enter the center dot.

In the diagram of Fig. 4(a), we observe that the transition voltage for electron relocalization into the center dot shifts to lower bias as N increases except for $N=3$ and $N=4$, which occurs at about −2.35 V. However, single electron charging occurs when the total energy for $N+1$ electrons $E_T(N+1)$ becomes lower than the total energy for N electrons $E_T(N)$, which is indicated by the vertical arrows on the diagram. At $V_{CCG}=-2.35$ V and $V_{CCG}=-2.2$ V, the third and fourth electrons, respectively, enter into the TQD system, by occupying the center dot, while the initial two electrons remain in the two side dots. Extrapolating from our simulation data, we infer that the addition of the first two electrons occurs at −3.6 and −3.165 V, respectively, which is outside the investigated voltage range.

In Fig. 5, we show 2D color plots of the ground-state electron densities for $N=2$, $N=3$, and $N=4$ configurations for various biases more negative than −2.2 V. As expected, in the stable configuration the first two electrons in the QDs form a singlet state [Fig. 5(a)]. Because the two electrons are physically decoupled (the separation of the density peaks between the two electrons is ∼0.6–0.7 μm), the singlet and triplet energies are very close to one another ($|\Delta E_{S\text{-}T}|<0.1$ meV). When the third electron enters the system at $V_{CCG}=-2.3$ V it occupies the center dot, forming a "spin density wavelike" state with two ↑ electrons in the two outer dots and a ↓ electron in the center dot [Fig. 5(b)].[25] Finally, when the fourth electron enters the system at $V_{CCG}=-2.25$ V, it is localized in the center dot to form a two-electron singlet state. We note that the center of mass of the two center electrons is now separated. The outer two QDs

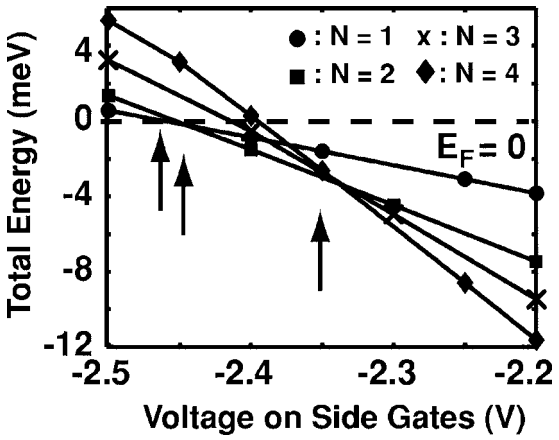

FIG. 6. Same as in Fig. 4(a) but with variation of the side gate bias.

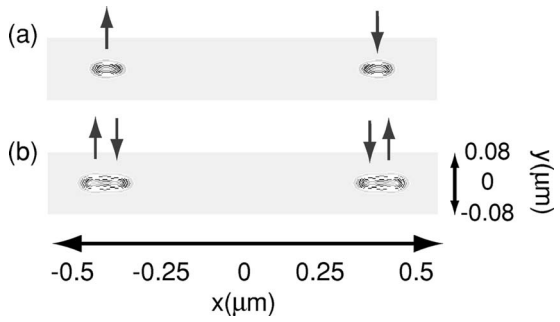

FIG. 7. Ground-state electron densities for (a) $N=2$ and (b) $N=4$ electrons. The arrows indicate the spin orientation. (SCG =side confining gate) (a) $V_{SSG}=-2.4$ V: the two electrons are localized in the two outer dots. (b) $V_{SCG}=-2.25$ V: two spin up electrons and two spin down electrons all localize in the side dots.

contain a spin ↑ (right dot) and a spin ↓ (left dot) electron, and there is a singlet in the center dot. However, wave functions in the center and side QDs do not overlap much here, so that the parallel spin configuration in the two side dots would result in practically the same energy [see Fig. 5(c)].

2. Side gate charging

Figure 6 shows the electron charging diagram for the first four electrons obtained by varying the voltage on the side confining gates (1) and (4) while keeping the center gates (2) and (3) constant, fixed at −2.4 V, and the tuning gates are set at −0.05 V throughout the simulations. Unlike the charging diagram in Fig. 4(a), here the total energy of the system is plotted against the two side confining gate biases (instead of the center gate biases). The confining gates are jointly varied, making the overall system again symmetric. Comparing our data now with the previous situation shown in Fig. 4(a), two differences emerge: (i) The "kinks" (very abrupt change in the slopes) associated with the relocalization of electrons from the side dots to the center dot are not present in this diagram since, because of the fixed negative center gate bias, all of the electrons just enter into the two side dots. In fact, this configuration is similar to a decoupled double quantum dot system since the uncharged center dot merely increases the separation between the two side dots. (ii) Instead of single-electron charging, we now observe double charging events for the third and fourth electrons. Let us mention that the occurrence of double charging for $N=3$ and $N=4$ is specific to the particular bias configuration of the center gates, which is within the range over which the side gate bias is swept.

The three charging points are again indicated by arrows in Fig. 6. At around $V_{SCG}=-2.44$ V, the curves $E_T(N=1)$, and $E_T(N=2)$ intersect each other just below the Fermi level at a single point. For $V_{SCG}<-2.46$ V, there are no electrons in the TQD as all curves for $N=1$, 2, 3, and 4 are above E_F. But at $V_{SCG}=-2.46$ V and $V_{SCG}=-2.44$ V the E_T curve for $N=1$ and $N=2$ become lowest, indicating the addition of the first and second electrons, respectively. As seen in Fig. 7(a), these nearly simultaneous charging events lead to one electron being in each of the two side dots, thereby making the Coulomb interactions between them negligible, below the numerical threshold of our model. At −2.34 V, three different total energy curves $E_T(N=2)$, $E_T(N=3)$, and $E_T(N=4)$ intersect one another at a single voltage value so that double charging (from $N=2$ to $N=4$) occurs here in the side dots [Fig. 7(b)], with the Coulomb interaction between the electrons in different dots remaining negligible. Hence, the TQD behaves as if the two side dots are decoupled. For the $N=2$ case, a spin ↑ electron and a spin ↓ electron occupy the two side dots, one in each dot, while for the $N=4$ case, two singlet state electrons occupy each of the side dots. In the latter configuration, the spin ↑ and the spin ↓ electrons overlap with one another in each of the side dots. But again, for this configuration a "broken-symmetry" state is seen in the separation of the center of mass of the spin density in each side dot.

C. Stability diagram

In Fig. 8, we show the stability diagram obtained from our simulation data by varying the biases on the two side (V_{SCG}) and the two center (V_{CCG}) confining gates and by keeping the tuning gate voltages constant. Four different curves can be seen, which distinguish regions with different numbers of electrons in the TQD system. An overlap of two different curves indicates electron double charging regions.

Overall, the stability diagram can be divided into two different regions. In the first region (-2.4 V$<V_{CCG}<-2.3$ V), the charging points are determined largely by the side gate voltages since all the electrons occupy the two outer dots. The weak V_{SCG} dependence is reflected in the slopes of the four curves ($\sim|0.07$ V/V$|$) in this region. Thus, the TQD system is largely indifferent to small changes in the V_{CCG}. In principle, we expect the electrons to double charge into the TQD if they enter into the side dots due to the structural symmetry. However, our simulation results show that this is not the case for the first two electrons since there exist a 10 mV separation between the first (solid dots) and second (solid square) electron curves. We attribute this artifact to the overestimated calculation of self-interaction energy for the first electron within the DFT formulation. However, for higher number of electrons, the self-interaction effects be-

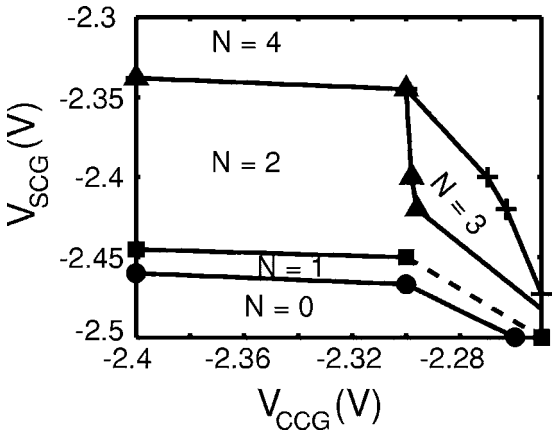

FIG. 8. Stability diagram for the first four electrons in the TQD. The solid dots, solid squares, solid triangles, and crosses depict curves separating stable charge regions between $N=0$ and $N=1$, $N=1$ and $N=2$, $N=2$ and $N=3$, and $N=3$ and $N=4$ electrons, respectively. Near the dotted segment in the "solid square" curve region, numerical nonconvergence occurs.

come negligible. Thus, we observe overlap of the third (solid triangle) and fourth (cross) electron curves in the first region.

In the second region ($V_{CCG} > -2.3$ V), the charging points are determined by both the V_{SCG} and the V_{CCG} since the electrons can now occupy all three dots. The absolute value of the slopes for all four curves is large and, in fact, becomes even larger for increasing positive values of V_{CCG}. Because of the absence of numerical convergence, the exact behavior of the second electron curve remains unknown and as such, is indicated by a dotted line. The separation between the third and fourth electron curves at $V_{CCG}=-2.3$ V indicates that the sole third electron enters into the central dot because of more favorable energy conditions, thereby moving away from the double-charging process. However, for higher V_{CCG} biases, the two curves merge again at a single voltage $V_{CCG} > -2.23$ V. At this point, the first two electrons are located in the central dot, leaving the side dots empty for double-charging.

V. CONCLUSION

We have provided a computer analysis of quantum confinement in, and orbital coupling between, three dots in a TQD structure for potential applications in quantum information processing. First, we showed that owing to the intrinsic nature of the colinearly coupled TQDs, the center dot is essentially different in character from the two side dots, requiring optimization of the whole mesa structure by eliminating unwanted effects that can be detrimental to practical device operation, in the few-electron or few-spin regime. Two different charging schemes have been investigated in order to provide a comprehensive analysis of the TQD electronic properties. At constant number of electrons, our simulations show electron onset of localization as a function of gate bias, which influences to various degrees the behavior of the total energy of the electron system with applied gate bias. Of particular interest are the onset of spin density wave-like state for $N=3$ electrons, and onset of localization in the center dot and two side dots for $N=4$ electrons, depending on the charging scheme, i.e., center gate charging or side gate charging. Finally, the stability diagram as a function of gate voltages V_{CCG} and V_{SCG} indicates a sizeable region within which "quasi" double charging occurs for $0 \rightarrow 2$ electrons and double charging for $2 \rightarrow 4$, with distinct features from the double dot system.

ACKNOWLEDGMENTS

This work was supported by ARO Grant No. DAAD 19-01-1-0659 under the DARPA-QUIST program and the Material Computational Center. The work performed at the Materials Computation Center was supported by the National Science Foundation under Grant No. DMR-03 25939 ITR, with additional support through the Frederick Seitz Materials Research Laboratory (U.S. Dept. of Energy Grant No. DEFG02-91ER45439) at the University of Illinois Urbana-Champaign. D.G.A. acknowledges help of A. Bezinger with device fabrication and G. Yu with autocad design.

[1] M. Nielsen and I. Chuang, *Quantum Computation and Quantum Information* (Cambridge University Press, Cambridge, England, 2000).
[2] L. K. Grover, Phys. Rev. Lett. **79**, 325 (1997).
[3] P. Shor, SIAM J. Comput. **26**, 1484 (1997).
[4] A. Barenco, C. H. Bennett, R. Cleve, D. P. DiVincenzo, N. Margolus, P. Shor, T. Sleator, J. A. Smolin, and H. Weinfurter, Phys. Rev. A **52**, 3457 (1995).
[5] D. Loss and D. P. DiVincenzo, Phys. Rev. A **57**, 120 (1998).
[6] D. S. Saraga and D. Loss, Phys. Rev. Lett. **90**, 166803 (2003).
[7] A. Vidan, R. M. Westervelt, M. Stopa, M. Hanson, and A. C. Gossard, Appl. Phys. Lett. **85**, 3602 (2004).
[8] P. Hawrylak and M. Korkusinski, Solid State Commun. **136**, 508 (2005).
[9] H. Sasakura, S. Adachi, S. Muto, T. Usuki, and M. Takatsu, Semicond. Sci. Technol. **19**, 409 (2004).
[10] W. G. van der Wiel, S. De Franceschi, J. M. Elzerman, T. Fujisawa, S. Tarucha, and L. P. Kouwenhoven, Rev. Mod. Phys. **75**, 1 (2003).
[11] R. Jones and O. Gunnarsson, Rev. Mod. Phys. **61**, 689 (1989).
[12] D. G. Austing (unpublished).
[13] T. Hatano, M. Stopa, and S. Tarucha, Science **309**, 268 (2005).
[14] D. G. Austing, T. Honda, and S. Tarucha, Semicond. Sci. Technol. **12**, 631 (1997).
[15] J. Kim, P. Matagne, J. P. Leburton, R. M. Martin, T. Hatano, and S. Tarucha, IEEE (unpublished).
[16] W. Kohn and L. J. Sham, Phys. Rev. **140**, 1133 (1965).
[17] J. P. Perdew and Y. Wang, Phys. Rev. B **45**, 13244 (1992).

[18] P. Matagne, J. P. Leburton, J. Destine, and G. Cantraine, Comput. Model. Eng. Sci. **1**, 1 (2000).
[19] R. G. Parr and W. Yang, *Density-Functional Theory of Atoms and Molecules* (Oxford University Press, London, 1989).
[20] M. Heath, *Scientific Computing: An Introduction Survey*, 2nd ed. (McGraw-Hill, New York, 2002).
[21] D. Jovanovic and J. P. Leburton, Phys. Rev. B **49**, 7474 (1994).
[22] K.-J. Bathe, *Finite Element Procedure in Engineering Analysis* (Prentice-Hall, Englewood Cliffs, NJ, 1982).
[23] J. C. Slater, *Quantum Theory of Molecules and Solids* (McGraw-Hill, New York, 1963).
[24] M. Leuenberger and D. Loss, Physica E (Amsterdam) **10**, 452 (2001).
[25] M. Koskinen, M. Manninen, and S. M. Reimann, Phys. Rev. Lett. **79**, 1389 (1997).